

Improvements in reverse breakdown characteristics of THz GaAs Schottky barrier varactor based on metal-brim structure

Lu-Wei Qi(祁路伟), Xiao-Yu Liu(刘晓宇), Jin Meng(孟进), De-Hai Zhang(张德海), Jing-Tao Zhou(周静涛)
Citation: Chin. Phys. B . 2020, 29(5): 057306 . **doi:** 10.1088/1674-1056/ab81fc
Journal homepage: http://cpb.iphy.ac.cn; http://iopscience.iop.org/cpb

What follows is a list of articles you may be interested in

Raman spectrum study of δ-doped GaAs/AlAs multiple-quantum wells

Wei-Min Zheng(郑卫民), Wei-Yan Cong(丛伟艳), Su-Mei Li(李素梅), Ai-Fang Wang(王爱芳), Bin Li(李斌), Hai-Bei Huang(黄海北)
Chin. Phys. B . 2018, 27(1): 017302 . **doi:** 10.1088/1674-1056/27/1/017302

Broadband microwave frequency doubler based on left-handed nonlinear transmission lines

Jie Huang(黄杰), Wenwen Gu(顾雯雯), Qian Zhao(赵倩)
Chin. Phys. B . 2017, 26(3): 037306 . **doi:** 10.1088/1674-1056/26/3/037306

Structural, electronic, and magnetic properties of transition-metal atom adsorbed two-dimensional GaAs nanosheet

Jia Luo(罗佳), Gang Xiang(向钢), Tian Yu(余天), Mu Lan(兰木), Xi Zhang(张析)
Chin. Phys. B . 2016, 25(9): 097305 . **doi:** 10.1088/1674-1056/25/9/097305

Heterogeneous integration of GaAs pHEMT and Si CMOS on the same chip

Li-Shu Wu(吴立枢), Yan Zhao(赵岩), Hong-Chang Shen(沈宏昌) You-Tao Zhang(张有涛), Tang-Sheng Chen(陈堂胜)
Chin. Phys. B . 2016, 25(6): 067306 . **doi:** 10.1088/1674-1056/25/6/067306

Field plate structural optimization for enhancing the power gain of GaN-based HEMTs

Zhang Kai, Cao Meng-Yi, Lei Xiao-Yi, Zhao Sheng-Lei, Yang Li-Yuan, Zheng Xue-Feng, Ma Xiao-Hua, Hao Yue
Chin. Phys. B . 2013, 22(9): 097303 . **doi:** 10.1088/1674-1056/22/9/097303

Improvements in reverse breakdown characteristics of THz GaAs Schottky barrier varactor based on metal–brim structure

Lu-Wei Qi(祁路伟)[1,2,3], Xiao-Yu Liu(刘晓宇)[2], Jin Meng(孟进)[1], De-Hai Zhang(张德海)[1], and Jing-Tao Zhou(周静涛)[2,†]

[1] *Key Laboratory of Microwave Remote Sensing, National Space Science Center, Chinese Academy of Sciences, Beijing* 100190, *China*
[2] *Institute of Microelectronics of the Chinese Academy of Sciences, Beijing* 100029, *China*
[3] *University of Chinese Academy of Sciences, Beijing* 100049, *China*

(Received 20 December 2019; revised manuscript received 10 March 2020; accepted manuscript online 23 March 2020)

The excellent reverse breakdown characteristics of Schottky barrier varactor (SBV) are crucially required for the application of high power and high efficiency multipliers. The SBV with a novel Schottky structure named metal–brim is fabricated and systemically evaluated. Compared with normal structure, the reverse breakdown voltage of the new type SBV improves from −7.31 V to −8.75 V. The simulation of the Schottky metal–brim SBV is also proposed. Three factors, namely distribution of leakage current, the electric field, and the area of space charge region are mostly concerned to explain the physical mechanism. Schottky metal–brim structure is a promising approach to improve the reverse breakdown voltage and reduce leakage current by eliminating the accumulation of charge at Schottky electrode edge.

Keywords: breakdown characteristics, Schottky metal–brim, Schottky barrier varactor, GaAs

PACS: 73.40.Mr, 73.61.Ey, 85.30.Kk, 42.65.Ky **DOI:** 10.1088/1674-1056/ab81fc

1. Introduction

The research of astrophysics and earth science is the primary motivator for the development of high output power and high efficiency terahertz sources.[1,2] Multiplier based on solid-state sources is the critical technology for generating power at terahertz frequency.[3,4] GaAs Schottky diodes are the core device of high output power multipliers due to its large electron mobility and uniform epitaxial material quality.[5,6]

In recent research, the edge field effect on the interface between Schottky metal and semiconductor causes a lower breakdown voltage and a larger leakage current.[7,8] This can induce lower power handling capability and poor conversion efficiency of multipliers.[9] A novel Schottky metal–brim structure (SMB) can effectively eliminate the accumulation of charge caused by edge-field effect, which will increase the output power of multipliers.

In this study, GaAs planner SBV with Schottky metal–brim structure (SMB-SBV) which is shown in Fig. 1(a) is fabricated and experimentally studied for the first time. Compared with normal SBV (normal-SBV), the SMB-SBV shows better breakdown characteristics (19.6% @ Schottky diameter is 3 μm). Combining the electric field and current density distribution extracted from simulations, the physical mechanism is discussed and explained.

2. Fabrication and simulation

The basic structures of the GaAs planner SBV are shown in Fig. 1. The epitaxial wafer is depicted as follows: a 30-μm-thick semi-insulating GaAs substrate serves as a supporting structure for the SBV devices; an epitaxial lattice-matched GaAs material including a 1.5-μm-thick heavily doped n-type GaAs layer (*i.e.*, n^+ GaAs buffer layer) and a 0.3-μm-thick lightly doped n-type GaAs layer (n-GaAs epi-layer), the doping concentrations of the two layers are $\sim 10^{18}$ cm^{-3} and $\sim 10^{17}$ cm^{-3}, respectively.

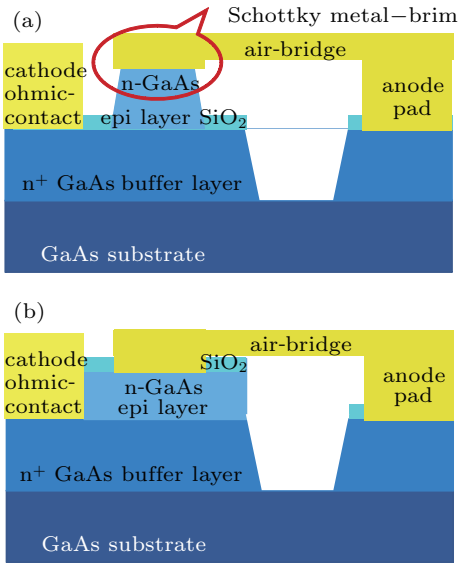


Fig. 1. Cross sectional schematic of GaAs SBV (a) Schottky metal–brim structure and (b) normal structure.

The fabrications start with mesa isolation using wet etching.[10] Ti/Au metal-layers are deposited by E-beam evaporation as anode Schottky contacts. Ni/Ge/Au cathode ohmic

†Corresponding author. E-mail: zhoujingtao@ime.ac.cn

© 2020 Chinese Physical Society and IOP Publishing Ltd

contacts are then deposited. After metal contacts are finished, SMB structure is formed by wet etching aided a certain power ultrasound. Then, samples are passivated with 300-nm SiO_2 and the dielectric layer existing on top of the metal contacts is removed by SF_6 dry etching. The process is completed with interconnection metal electroplate to form gentle air bridge. Based on this SMB-SBV, the 225-GHz millimeter-wave integrated circuits (MMIC) are also produced. Figure 2(a) shows three anodes series GaAs SBVs and figure 2(b) shows the details of the SMB structure. The diameter of Schottky anodes in this paper is 3 μm. A Schottky anode with a diameter of 40 μm is also designed to analyze the physical mechanism of the SMB structure.

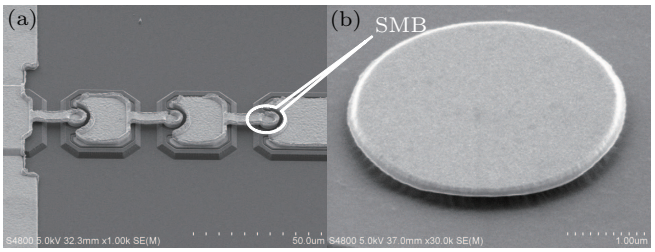


Fig. 2. Scanning electron microscope (SEM) photographs of (a) the fabricated GaAs SBVs, (b) Schottky metal–brim structure details.

The electrical simulations described in this paper are performed using Sentaurus TCAD tools.[11] The simulations with metal–interfacial layer–semiconductor (MIS) model which is shown in Fig. 3 are based on the literature in Refs. [12,15]. In the simulation, the two-dimensional (2D) structures are depicted in Fig. 1 and the doping levels are described above. Adequate numerical convergence is also reached by an optimized meshing, with nanometer grid spacing for the key electrical layers and their interfaces. The model is based on the basic drift-diffusion and Poisson equations for direct current (DC), breakdown characteristics, and small signal simulation.[13,14] The drift-diffusion for electrons and Poisson equations are given respectively by

$$J_n = q\mu_n\left(n\nabla V - 1.5nkT\nabla \ln m_n\right) + qD_n\left(\nabla n - n\nabla \ln \gamma_n\right), \quad (1)$$

$$\nabla\cdot(\varepsilon\nabla\phi + \boldsymbol{P}) = -q\left(p - n + N_{\rm D} - N_{\rm A}\right) - \rho_{\rm trap}, \quad (2)$$

where J_n is the electron current density, μ_n is mobility, n is electron density, p is hole density, m_n is electron effective mass, γ_n is Boltzmann statistics, ε is electrical permittivity, ϕ is the electrostatic potential, $\boldsymbol{P}$ is the ferroelectric polarization, $N_{\rm D}$ and $N_{\rm A}$ are the concentrations of ionized donors and acceptors, q is the electron charge, k is the Boltzmann constant, T is the temperature.

This basic drift-diffusion model includes Fermi statistics, mobility with doping dependence and high velocity saturation model, carrier generation, and recombination, non-local tunneling, and band to band tunneling.

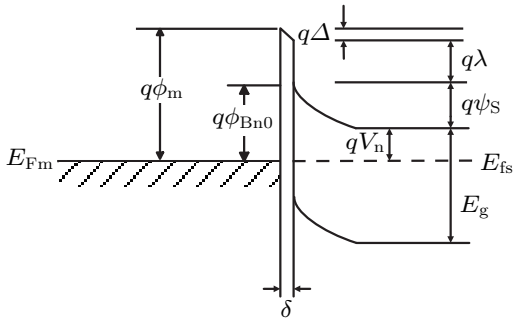


Fig. 3. Energy band diagram of MIS model.

3. Measurement methods

The forward I–V and reverse breakdown characteristics are measured with Agilent 4200 semiconductor parameter analyzer at room temperature. S-parameters is also measured by Agilent E8363B network analyzer to extract depletion layer capacitance. The test frequency range is 0.1 GHz–40 GHz. According to Taking's studies in Ref. [16] the SBV is embedded in the ground–signal–ground (GSG) coplanar waveguide to measure the S-parameters of the coplanar waveguide. Three auxiliary structures, diode-open, diode-short, and pin-open are used to obtain the junction capacitance at 0-V bias ($C_{\rm j0}$) by using the single-port open-short de-embedding method. Figure 4 shows the equivalent circuits of the three structures based on the work in Ref. [17]. Figure 5 shows the photograph and equivalent circuit of the actual SBV. The pad-to-pad capacitance $C_{\rm pp}$, the finger-to-pad capacitance $C_{\rm fp}$, the finger inductance $L_{\rm f}$, and the finger resistance $R_{\rm f}$ are the parasitic parameters. $C_{\rm j}$ is the intrinsic voltage-dependent junction capacitance. $R_{\rm s}$ is the series resistance.

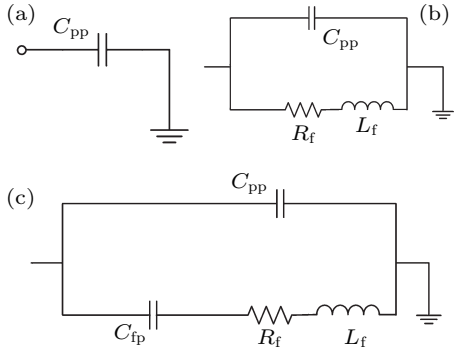


Fig. 4. The equivalent circuit of (a) diode-open, (b) diode-short, and (c) pin-open structure.

Under small-signal conditions (at an input power of −20 dBm), the magnitude and phase of the S-parameters are measured, which could directly convert to Y-parameters. The steps of extracting $C_{\rm j0}$ are as follows:

(i) In diode-open structure, $C_{\rm pp}$ is determined by

$$Y_{\rm diode-open} = -{\rm j}wC_{\rm pp}. \quad (3)$$

(ii) In diode-short structure, L_f and R_f are determined by

$$jwL_f = \frac{1}{Y_{diode-short} - Y_{diode-open}}, \tag{4}$$

$$R_f = re\left(\frac{1}{Y_{diode-short} - Y_{diode-open}}\right). \tag{5}$$

(iii) In pin-open structure, C_{fp} is determined by

$$\frac{1}{jwC_{fp}} = \frac{1}{Y_{pin-open} - Y_{diode-open}} - \frac{1}{Y_{diode-short} - Y_{diode-open}}. \tag{6}$$

(iv) The obtained C_{pp}, L_f, R_f, and C_{fp} are substituted into the equivalent circuit model of SBV which is shown in Fig. 5(b). The C_{j0} is obtained by fitting the simulation results of S-parameters to the measurement results.

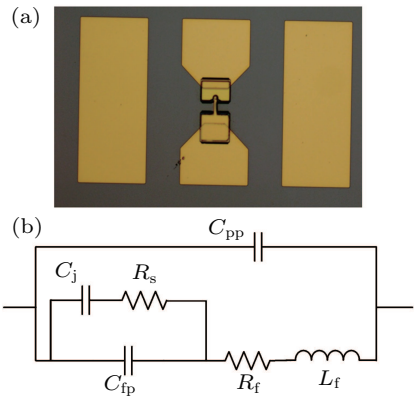


Fig. 5. (a) Photograph and (b) equivalent circuit of the actual SBV.

4. Result and discussion

According to the thermal electron emission model,[15] the current–voltage curve across the Schottky diode can be described by

$$I(V) = I_0\left[\exp\left(\frac{qV}{nkT}\right) - 1\right], \tag{7}$$

where I_0 is the reverse saturated current, n is ideal factor.[18]

Figure 6 shows the forward I–V characteristics in a log scale and the turn-on voltage is 0.68 V as measured at a current of 1 μA. The ideal factor is a figure of merit that describes an unnecessary current path except the thermionic electron emission current, which is induced by interfacial disorder, interface state densities, electron tunneling current.[19–21] The ideal factor is defined as

$$n = \frac{q}{kT}\frac{dV}{d\ln(I)}. \tag{8}$$

By numerical fitting using formula (3), the ideal factor (n) and the effective barrier height ($\phi(V)$) could be calculated. The series resistance (R_s) is also extracted based on the report in Ref. [22], which is shown in Table 1. The SMB-SBV has a similar ideal factor, series resistance, and barrier height as normal-SBV.

The breakdown characteristics with different structures of SBV are shown in Fig. 7. In order to investigate the improvements in reverse breakdown characteristics of SMB-SBV, a current of 1 μA for defining the breakdown voltage of SBV is used.[23] The GaAs SBV with different structures has the breakdown voltage of the order of −8.75 V for SMB structure and −7.31 V for normal one, respectively. The results show that SMB-SBV has the advantage of high breakdown voltage. The leakage current caused by electron tunneling is significantly lower than that of normal-SBV. Simulated results based on the MIS model and measurement results show a good agreement as shown in Figs. 6 and 7. So, multipliers based on SMB-SBV will have larger power handling capability and better power conversion efficiency.

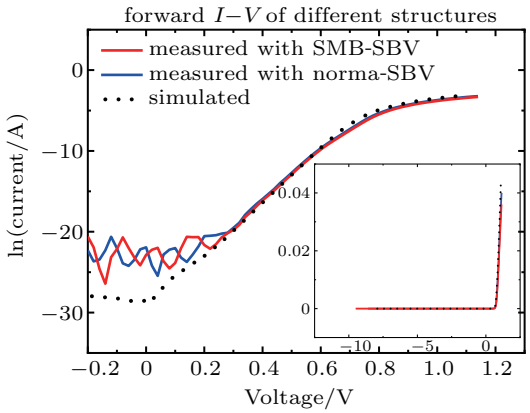


Fig. 6. Forward I–V characteristics with different structures in log scale; full line: measured; dashed line: simulated. The inset shows the I–V in linear scale.

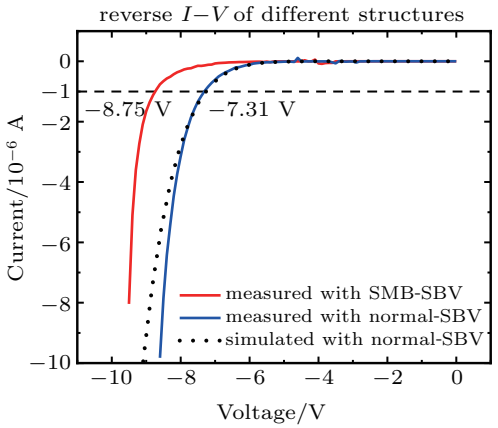


Fig. 7. Variations of breakdown characteristics with different structures.

Furthermore, the breakdown characteristics of SBVs with a Schottky junction diameter of 40 μm are shown in Fig. 8. Due to the large difference of anode area, the normalized current density is used to compare the influence of the edge electric field effect of different areas on the breakdown characteristics. The current value corresponding to the same current

density is marked in Fig. 8. It shows that the breakdown voltage is −7.29 V for SMB structure and −6.75 V for normal structure at the same order of leakage current density. It reveals that the improvements in reverse breakdown characteristics of SMB structure obviously decreases with the increasing of anode area. Accordingly, SMB structure might increase the utility of SBV for THz multipliers where the anode area must be decreased in order to achieve greater application frequency.

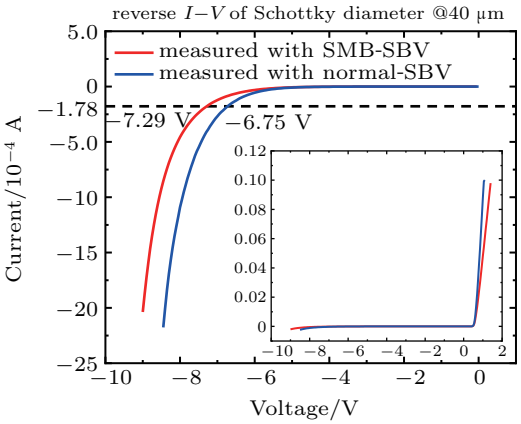


Fig. 8. Variations of breakdown characteristics with different structures at Schottky diameter of 40 μm. The inset shows the *I*–*V* curve in linear scale.

The measurement and fitting data of the *S*-parameters are shown in Fig. 9, and they are in good agreement. The extracted junction capacitance at 0-V bias (C_{j0}) is 13.7 fF for SMB structure and 16.5 fF for normal structure, respectively. The C_{j0} of SMB-SBV is less than that of normal structure, which shows a larger capacitance modulation ratio (C_{max}/C_{min}). The SMB-SBV shows better conversion efficiency because of its uniform capacitance modulation ration.

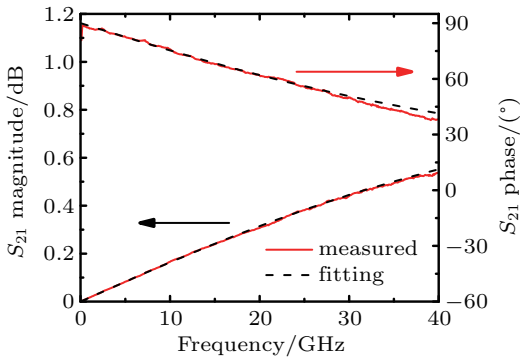


Fig. 9. Measurement and fitting data of S_{21} at the frequency range of 0.1 GHz–40 GHz.

Table 1. Parameters of SBVs with different structures.

Parameters	SMB-SBV	Normal-SBV
Diameter/μm	3	3
Ideal factor	1.14	1.15
Breakdown voltage/V	−8.75	−7.31
C_{j0} by *S*-parameter/ fF	13.7	16.5
R_s/Ω	5.4	5.3
Reverse saturation current/A	1.14×10^{-13}	1.75×10^{-13}
Junction potential/V	0.69	0.69

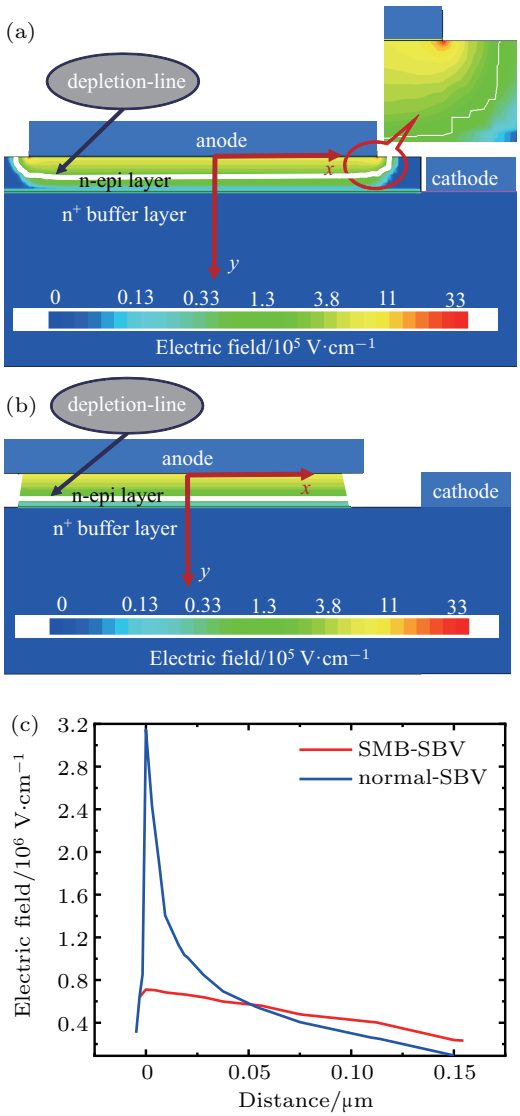


Fig. 10. Depletion layer area (white line) and electric field distribution near the edge of the anode metal of (a) normal-SBV, (b) SMB-SBV, (c) cross-section of the electric field distribution.

In order to investigate the physical mechanism of SMB with excellent reverse breakdown characteristics, simulations are carried out to precisely extract the distribution of electric field and space charge area at the same reverse bias voltage. The difference between the depletion layer region and the electric field distribution of these two structures is shown in Fig. 10. At the edge of the anode electrode, the maximum electric field of normal structure is approximately 4.5 times of the SMB structure one, which suffers from the electric field crowding near the metal edge. This would induce local breakdown in advance, especially happened between the anode and cathode region.[24] From Fig. 11, it is obvious that the leakage current mainly comes from the edge of the depletion layer. The normal SBV has a narrow depletion layer near the edge of the anode electrode. It causes an increase in C_{j0} calculated from the formula as a function of C_{j0}

$$C_{j0} = \gamma\varepsilon\frac{A_a}{W_{bi}}, \quad \gamma = 1 + \frac{bW_{bi}}{r_a}, \tag{9}$$

where W_{bi} is zero bias depletion width, γ is fringing capacitance factor. A_a is the area of anode.[20]

The SMB structure provides electric field relief and uniform depletion layer distribution, reducing the magnitude of the electric field. The SMB-SBV shows excellent electrical performance because it completely eliminates the accumulation of charge at Schottky electrode edge.

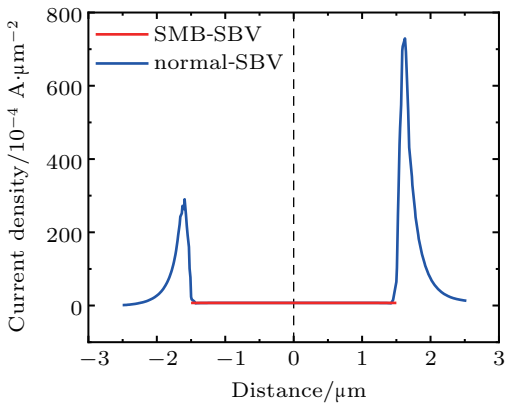


Fig. 11. Distribution of leakage current density across the anode depletion layer. The abscissa corresponds to the horizontal depletion layer distribution (x axis in Fig. 10) and the dotted line is the center of the anode.

5. Summary

In summary, the GaAs SBV with SMB structure is fabricated and systemically evaluated. With SMB structure, the reverse breakdown voltage increases from −7.31 V to −8.75 V. The C_{j0} is reduced from 16.5 fF to 13.7 fF due to SMB structure ignoring the fringe capacitance factor. SMB structure would not cause the degradation of other SBV characteristics, such as ideal factor, reverse saturation current, and series resistor. The distributions of the leakage current and the electric field are extracted by Sentaurus TCAD tools, which reveal that SMB structure can eliminate the accumulation of charge at Schottky electrode edge induced by edge-field effect. The reverse breakdown voltage will be larger if SMB etching process is optimized. Through a series of comparisons, the GaAs SBV with SMB structure shows significantly better electrical characteristics including larger breakdown voltage, lower leakage current, and larger capacitance modulation ratio, which is beneficial to high power and high efficiency multipliers application.

References

[1] Chattopadhyay G 2011 *IEEE Trans. Terahertz Sci. Technol.* **1** 33
[2] Marso M 2010 *The Eighth International Conference on Advanced Semiconductor Devices and Microsystems* p. 147
[3] Dhillon S S, Vitiello M S, Linfield E H, Davies A G, Hoffmann M C and Booske J 2017 *J. Phys. D: Appl. Phys.* **50** 043001
[4] Mittleman D M 2018 *Opt. Express* **26** 9417
[5] Hou D, Chen J and Yan P 2018 *IEEE Trans. Terahertz Sci. Technol.* 1
[6] Martin S, Nakamura B, Fung A, Smith P, Bruston J and Maestrini A 2001 *IEEE MTT-S International Microwave Sympsoium Digest* p. 1641
[7] Lewis J A and Wasserstrom E 1970 *Bell Syst. Tech. J.* **49** 1183
[8] Huang Y, Jayaprakash K V A and Cheung C 2014 *IEEE Applied Power Electronics Conference and Exposition-APEC* p. 2902
[9] Liang S, Song X, Zhang L, Lv Y, Wang Y, Wei B and Feng Z 2020 *IEEE Electron Dev. Lett.* 1
[10] Liu X Y, Zhang Y, Xia D J, Ren T H, Zhou J T, Guo D and Jin Z 2017 *Chin. Phys. Lett.* **34** 070701
[11] Schwarz M and Kloes A 2016 *IEEE Trans. Electron Devices* **63** 2757
[12] Nawawi A, Tseng K J, Amaratunga G A J, Umezawa H and SHikata S 2013 *Diamond Relat. Mater.* **35** 1
[13] Goossens R J G, Beebe S, Yu Z and Dutton R W 1994 *IEEE Transactions on Computer-Aided Design of Integrated Circuits and Systems* p. 310
[14] Trojnar A H, Valdivia C E and LaPierre R R 2016 *IEEE Journal of Photovoltaics* **6** 1494
[15] Neamen and Donald A 2003 *Semiconductor physics and devices: basic principles* (NY: McGraw-Hill) p. 212
[16] Taking S 2012 *AlN/GaN MOS-HEMTs technology* Doctoral dissertation (Glasgow: University of Glasgow)
[17] Ren T, Zhang Y, Liu S, Guo F, Jin Z, Zhou J and Yang C 2017 *J. Infrared, Millimeter, Terahertz Waves* **38** 143
[18] Tang A Y, Drakinskiy V, Sobis P, Vukusic J and Stake J 2009 *34th International Conference on Infrared, Millimeter, and Terahertz Waves* p. 1
[19] Ellis J A and Barnes P A 2000 *Appl. Phys. Lett.* **76** 124
[20] McLean A B, Dharmadasa I M and Williams R H 1986 *Semicond. Sci. Technol.* **1** 137
[21] Maeda K, Ikoma H, Sato K and Ishida T 1993 *Appl. Phys. Lett.* **62** 2560
[22] Kiuru T, Mallat J, Raisanen A V and Narhi T 2011 *IEEE Trans. Microwave Theor. Techniq.* **59** 8
[23] Saini K S 2003 *Development of frequency multiplier technology for ALMA*
[24] Narita T, Kikuta D, Takahashi N, Kataoka K, Kimoto Y, Uesugi T and Sugimoto M 2011 *Phys. Status Solidi A* **208** 1541